nature chemical biology

ARTICLE

PUBLISHED ONLINE: 8 AUGUST 2016 | DOI: 10.1038/NCHEMBIO.2145

FRET binding antenna reports spatiotemporal dynamics of GDI–Cdc42 GTPase interactions

Louis Hodgson[1–4,8*], Désirée Spiering[1,2,8], Mohsen Sabouri-Ghomi[5], Onur Dagliyan[3,4], Céline DerMardirossian[6], Gaudenz Danuser[5,7*] & Klaus M Hahn[3,4*]

Guanine-nucleotide dissociation inhibitors (GDIs) are negative regulators of Rho family GTPases that sequester the GTPases away from the membrane. Here we ask how GDI–Cdc42 interaction regulates localized Cdc42 activation for cell motility. The sensitivity of cells to overexpression of Rho family pathway components led us to a new biosensor, GDI.Cdc42 FLARE, in which Cdc42 is modified with a fluorescence resonance energy transfer (FRET) 'binding antenna' that selectively reports Cdc42 binding to endogenous GDIs. Similar antennae could also report GDI–Rac1 and GDI–RhoA interaction. Through computational multiplexing and simultaneous imaging, we determined the spatiotemporal dynamics of GDI–Cdc42 interaction and Cdc42 activation during cell protrusion and retraction. This revealed remarkably tight coordination of GTPase release and activation on a time scale of 10 s, suggesting that GDI–Cdc42 interactions are a critical component of the spatiotemporal regulation of Cdc42 activity, and not merely a mechanism for global sequestration of an inactivated pool of signaling molecules.

Rho GTPases are critical in numerous cell functions, but they are especially well characterized in the regulation of cytoskeletal dynamics[1–3]. GTPases are activated via binding of a GTP nucleotide and deactivated via hydrolysis of GTP to GDP. Their molecular mechanisms and effector pathways have been determined through structural analysis, biochemical approaches and imaging. However, only through the implementation of biosensors that report GTPase activity *in situ* has it become clear that GTPase cycles are modulated on length and time scales of single micrometers and seconds[4–9].

Three families of regulatory proteins modulate Rho GTPase activity: guanine-nucleotide exchange factors (GEFs) facilitate removal of GDP and binding of GTP, and GTPase-activating proteins (GAPs) accelerate the hydrolysis of bound GTP to GDP. GDIs sterically block effector interactions and extract GTPases from the membrane to prevent activation by GEFs. More than 80 GEFs and GAPs act on Rho GTPases[10]. This diversity confers specificity, enabling a wide variety of input signals to generate different cell behaviors via a relatively small number of Rho GTPases (22 Rho family members in mammals, of which Cdc42, Rac1 and RhoA have been most prominently implicated in cytoskeletal regulation). Initial evidence using GTPase biosensors and other approaches suggests that GEFs and GAPs generate this wide variety of cell behaviors by controlling the location and kinetics of GTPase activation.

In contrast to the GEFs and GAPs, there are only three genes encoding RhoGDIs, and each of their protein products interacts with several GTPases. Among them, RhoGDI1 (or RhoGDIα, hereinafter referred to simply as GDI) is the most abundant and ubiquitously expressed isoform, and it interacts with all three canonical GTPases. Accordingly, it has been assumed that GDI–GTPase interactions are less specific and less spatially regulated, functioning primarily to provide a uniform cytosolic pool of inactive GTPases that can be accessed by localized regulatory proteins. However, some studies have suggested that there is a certain degree of spatiotemporal regulation of GDI–GTPase interactions, mediated by lipids[11–13] and kinases that control GDI–GTPase affinity by phosphorylating RhoGDI[14–17] or the GTPase[18–21]. Therefore, it is plausible that modulation of GDI–GTPase interactions also contributes to the fine-tuned spatiotemporal organization of Rho GTPase signaling.

To address the question of how much GDI–GTPase interactions contribute to the regulation of GTPase activity, we focused on developing biosensors that could report the localization and concentration of GDI–GTPase complexes in living cells. We developed a new biosensor design based on a 'binding antenna', a single chain containing two fluorescent proteins (FPs) attached to the GTPase of interest. The FRET efficiency of the binding antenna is altered when GDI binds to the GTPase. An important advantage of this design for our work was its ability to reduce the need to introduce exogenous protein. The biosensor reports interaction between modified Cdc42 and endogenous GDI. With the GDI–GTPase biosensor, we explored changes in the distribution of GDI–Cdc42 complex during motility. Far from being a uniform reservoir of inactive GTPase, the GDI–GTPase complex concentrated in protrusions at precise times and positions relative to edge movement and relative to nearby Cdc42 activation. To test how GDI–Cdc42 complex formation affects Cdc42 activation, we modified our existing dye-based biosensor of Cdc42 activity (meroCBD)[6] and imaged GDI–Cdc42 interaction and Cdc42 activity concurrently in the same cell. To our knowledge, this paper presents the first spatiotemporally resolved map of GDI-mediated Cdc42 regulation.

RESULTS

A fluorescent biosensor of GDI–Cdc42 binding

The design of the new GDI–Cdc42 interaction biosensor stemmed from biosensor optimization studies in which we discovered that FRET between two FPs attached to the N terminus of Cdc42 responded strongly to interaction with wild-type, 'unlabeled' GDI (**Fig. 1a**). The binding antenna attached to Cdc42's N terminus

[1]Department of Anatomy and Structural Biology, Albert Einstein College of Medicine, Bronx, New York, USA. [2]Gruss-Lipper Biophotonics Center, Albert Einstein College of Medicine, Bronx, New York, USA. [3]Department of Pharmacology, University of North Carolina at Chapel Hill, Chapel Hill, North Carolina, USA. [4]Lineberger Cancer Center, University of North Carolina at Chapel Hill, Chapel Hill, North Carolina, USA. [5]Department of Cell Biology, The Scripps Research Institute, La Jolla, California, USA. [6]Department of Immunology and Microbial Science, The Scripps Research Institute, La Jolla, California, USA. [7]Department of Cell Biology, Harvard Medical School, Boston, Massachusetts, USA. [8]These authors contributed equally to this work. *e-mail: louis.hodgson@einstein.yu.edu, Gaudenz.Danuser@UTSouthwestern.edu or khahn@med.unc.edu

consisted of monomeric Cerulean (mCer)[22] attached via an optimized short linker to circularly permuted Venus[23]. The mCer contained an A206K mutation to reduce interaction between the FPs[24]. By optimizing the antenna structure using different linkers and circular permutants (**Supplementary Results**, **Supplementary Fig. 1**), we were able to generate a structure that responded effectively to GDI but not to GEFs, GAPs or Cdc42 effectors. GTPases require post-translational modification with a lipid moiety at the C terminus for GDI binding (the lipid binds to the immunoglobulin-like β-sandwich of the GDI)[25]. Thus, to maintain normal GDI functions it was essential to keep the GTPase C terminus intact. We named the new biosensor GDI.Cdc42 FLARE. Although we focus here on Cdc42–GDI interactions, we also produced biosensors for Rac1–GDI and RhoA–GDI interactions (**Supplementary Figs. 1** and **2**); biological studies with these will be pursued in the future.

We assayed the specificity and fluorescence response of the biosensor by obtaining fluorescence spectra of biosensor mutants coexpressed with different Cdc42 upstream regulators in suspensions of HEK 293T cells. The use of increasing ratios of regulator to biosensor cDNA revealed plateaus in fluorescence change, indicating where binding and the resulting effects on fluorescence saturated, similar to previous results[5]. We observed a 218% increase in FRET:CFP emission ratio when we increased the amount of GDI from no expression to a 4:1 GDI:biosensor cDNA ratio. We also examined the fluorescence of the biosensor and its mutants with and without coexpression of excess GDI (**Fig. 1b**,**c**). Only mutants capable of binding to GDI showed effects of GDI coexpression. The R66E mutant, deficient in GDI binding, showed no change in FRET with or without excess GDI. The D118 mutant, unable to release GEFs, showed no fluorescence change with or without excess GDI, indicating that the biosensor did not respond to GEF binding. This mutation also prevented response to GDI, consistent with previous data indicating competition between GEFs and GDI for the same binding regions on GTPases[2,10]. Effector binding did not affect FRET, as the T35S mutant, which blocks effector binding[26,27], did not alter the response to GDI. Furthermore, there was no response to either coexpressed GEFs or downstream effectors (**Supplementary Fig. 3a**,**b**).

The coexpression of exogenous, activated GEFs abrogated FRET response to excess GDI (**Fig. 1d**), but only for GEFs that affect Cdc42 (the RhoA GEF Ect2 does not bind Cdc42). Reduction of the FRET response caused by fourfold excess GDI required a fourfold excess of GEF relative to biosensor cDNA, consistent with GEF–Cdc42 affinities and previously published results[5]. Excess GEFs alone had no effect on biosensor fluorescence, nor did GAPs (**Fig. 1d**). In these experiments we used constitutively active DH-PH fragments of GEFs (**Fig. 1d**). We obtained similar results with full-length GEFs (**Supplementary Fig. 3a**,**b**) using T17N and D118A Cdc42 mutants that are known to tightly sequester GEFs[28].

The biosensor's remarkable selectivity for GDI is consistent with published crystal structures. The cp49 variant of the Venus FP extends from Cdc42 at a position that is not part of the known binding sites for GEFs, GAPs, GDI or effectors (**Supplementary Fig. 4**). There was almost no FRET when the biosensor was free of GDI, as indicated by biosensor FRET with and without GDI coexpression (**Fig. 1b**) and by the dependence of FRET on intracellular concentration (**Supplementary Fig. 5a**; biosensor FRET plateaued at a low value when increasing expression levels decreased binding to endogenous GDI). Low FRET was not due to proteolysis, as shown by gel electrophoresis (**Supplementary Fig. 5b**). The low FRET in the GDI-free state indicated that the two FPs adopted a relatively fixed conformation in which their distance and/or orientation produced little FRET. The two FPs may have been in a low-FRET conformation as a result of steric and torsional factors, or because mCer bound to a portion of the Cdc42 surface accessible only when the sensor was GDI free (**Supplementary Fig. 4**). mCer may interact with the region where GDI binds to the C-terminal tail

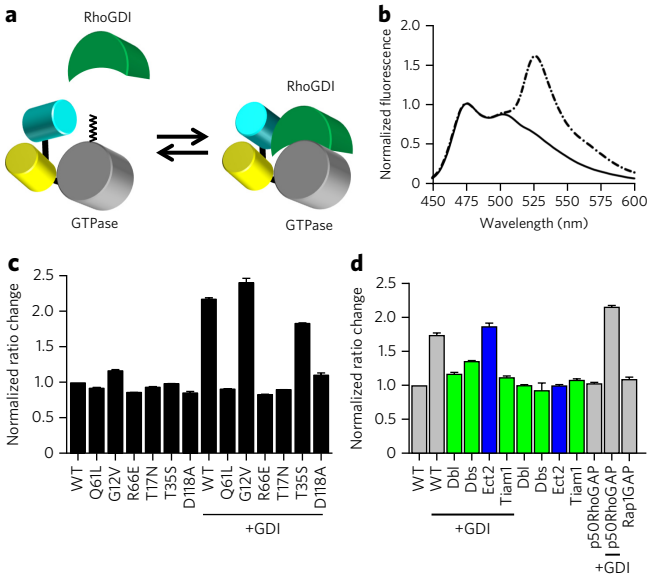

Figure 1 | Design and validation of GDI.Cdc42 FLARE, a genetically encoded biosensor that reports localization of GDI–Cdc42 complexes. (**a**) The FRET of a binding antenna on Cdc42 is altered when Cdc42 binds endogenous GDI. (**b**) Representative, normalized emission spectra of GDI.Cdc42 FLARE in HEK 293T cells (excitation, 433 nm; normalized at the 474-nm emission peak). Solid line, biosensor; dashed-dotted line, biosensor plus excess GDI. (**c**) Normalized FRET/CFP emission ratios of GDI.Cdc42 FLARE mutant biosensors, expressed with and without excess GDI. (**d**) Normalized FRET/CFP emission ratios of GDI.Cdc42 FLARE with coexpressed GEFs or GAPs, in the presence or absence of excess GDI. Green bars indicate Cdc42-interacting GEFs. Blue bars indicate GEFs that do not interact with Cdc42. For **b**–**d**, results shown are the mean of three independent measurements. Error bars represent s.e.m. WT, 'wild type' (i.e., the sensor without any introduced mutation).

of Cdc42, and where GEFs, GAPs and effectors do not bind. FRET increased upon GDI binding, but this FRET diminished when we reduced interactions between the FPs by adding an A206K mutation[24] into circularly permuted Venus (**Supplementary Fig. 5c**). This suggested that interactions between the FPs enhanced FRET in the GDI-bound state. Interaction of the FPs with GDI may also induce a high FRET conformation.

Dynamics of the GDI–Cdc42 complex in cell protrusions

We stably expressed the GDI.Cdc42 FLARE biosensor in mouse embryonic fibroblasts (MEF/3T3) under the control of a tetracycline-inducible promoter (tet-OFF) as described previously[5]. The cells were sensitive to overexpression of the biosensor, as they are to overexpression of Cdc42 (ref. 6). We therefore established stable, inducible cells with levels of biosensor expression below those producing effects on cell morphology or motile behavior (**Supplementary Fig. 6**). The biosensor showed elevated binding of GDI to Cdc42 throughout most of the cell body, but cell edges showed reduced FRET/donor ratios, indicating that the majority of the GDI–Cdc42 complex occupied the bulk cytosolic space in the cell body (**Fig. 2a**). Live-cell imaging of the GDI–Cdc42 complex showed strikingly dynamic behavior at the cell edge during protrusion–retraction cycles (**Fig. 2b**, **Supplementary Videos 1**–**4**). Line scans perpendicular to the cell edge showed reduced FRET ratios within 2 μm of the edge during protrusion, whereas the ratio increased during retraction, with the highest values associated with ruffles undergoing retrograde movement (**Fig. 2b**). This indicated that amounts of GDI–Cdc42 complex decreased specifically at the edge during protrusion and concentrated in rearward-moving

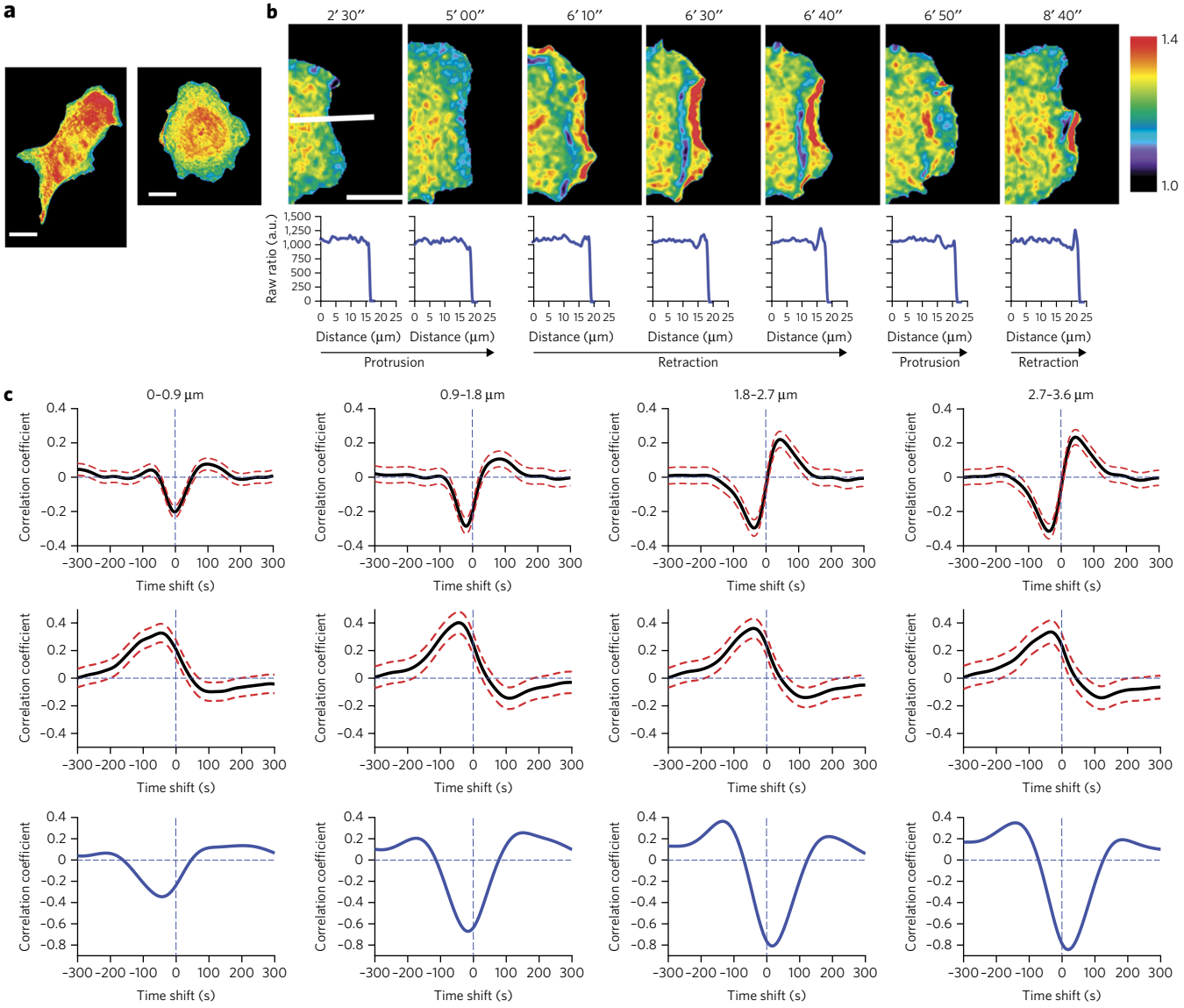

Figure 2 | GDI–Cdc42 complex localization in living cells. (**a**) MEFs expressing the GDI.Cdc42 FLARE biosensor. Note the relatively uniform distribution of GDI–Cdc42 complex except at the cell edges. Scale bars, 10 μm. (**b**) Localization of GDI–Cdc42 at the edge of a cell undergoing protrusion–retraction cycles. Below each image is the fluorescence ratio measured along the white line shown in the first image. The amount of GDI–Cdc42 complex decreased at the cell edge during protrusion and increased during retraction. a.u., arbitrary units. (**c**) Top row: correlation of GDI–Cdc42 localization and edge velocity, measured using the GDI.Cdc42 FLARE biosensor. Correlation curves were computed from $n = 704$ individual windows in eight cells (**Supplementary Fig. 6**). Middle row, correlation of Cdc42 activity and edge velocity measured in wild-type MEFs using the meroCBD biosensor. Correlation curves were computed from $n = 420$ individual windows in seven cells. Bottom row, cross-correlation of the correlation curves shown in the top and middle rows. Number ranges above the graphs indicate the distance from the cell edge.

ruffles during retraction. The ruffles showed reduced amounts of GDI–Cdc42 complex on the side distal from the edge.

To investigate the dynamics of GDI–Cdc42 binding more quantitatively, we used cross-correlation between the FRET/donor ratio and cell edge motion, as used previously to analyze coupling of GTPase activities with cell edge velocity[4]. We first verified that the average periods of protrusion–retraction cycles in parental mouse embryonic fibroblasts (MEFs) and those expressing GDI.Cdc42 FLARE biosensor were statistically indistinguishable (**Supplementary Fig. 6**). This confirmed that biosensor expression did not perturb the regulation of basal protrusion–retraction cycles. Consistent with the line scan analysis (**Fig. 2b**), the coupling between GDI–Cdc42 and edge motion in sampling windows subadjacent to the leading edge (0–0.9 μm) showed substantial negative cross-correlation (-0.203 ± 0.034; 95% confidence about the mean; $P = 0.0261$, t-test of H_0: correlation peak = 0) at a time lag of -2 ± 13 s (**Fig. 2c**). This suggested that overall GDI–Cdc42 binding decreased concurrently with edge protrusion and increased during retraction. The strength of this negative correlation increased to a highly significant value at the next sampling window position (0.9–1.8 μm from the edge; $P = 0.0016$, t-test of H_0: correlation peak = 0), and the negative time lag also increased (-20 ± 9 s) (**Fig. 2c**). This indicated that the modulation of GDI–Cdc42 interaction slightly lagged the modulation of edge velocity. In sampling windows even farther from the edge, a significant positive cross-correlation peak appeared at 42 ± 23 s (at 1.8–2.7 μm, $P = 0.0159$; at 2.7–3.6 μm, $P = 0.0106$; t-tests of H_0: correlation peak = 0) (**Fig. 2c**). The strength of this positive peak increased with the distance to the cell edge, indicating increased GDI–Cdc42 binding before protrusion and/or GDI–Cdc42 release before retraction. Together these analyses revealed

distinct, fine-tuned regulation of GDI–Cdc42 binding for different regions at the cell edge.

Next, we wished to understand GDI–Cdc42 dynamics relative to Cdc42 activation. We decided to approach this first by computational multiplexing (**Supplementary Fig. 7**), in which we measured the kinetics of biosensor activities in separate cells and determined their relationship to cell edge motion, which was used as a common fiduciary[4]. As previously reported[6], we monitored Cdc42 activity in wild-type MEFs using meroCBD. Consistent with our previous analyses[4], we found significant correlation between Cdc42 activation and edge velocity at a time lag of −46 ± 31 s ($P = 10^{-5}$, *t*-test of H_0: correlation peak = 0) (**Fig. 2c**), indicating delayed Cdc42 activation relative to cell protrusion. Also consistent with our previous findings, the correlation between edge velocity and Cdc42 activity was maximal in the window row 0.9–1.8 μm from the cell edge, suggesting that Cdc42 probably activated at the location of mature focal adhesions, which were, on average, 2–3 μm back from the cell edge (**Fig. 2c**). Beyond the second row of windows, the correlation strength decreased. Qualitatively, these Cdc42 activation characteristics matched well with our observation of a negative correlation peak between edge motion and GDI–Cdc42 interaction at −20 s to −40 s. This suggested that the negative correlation between edge motion and GDI–Cdc42 binding was associated predominantly with a release of Cdc42 from GDI shortly after protrusion onset. To confirm this relationship more systematically, we computed the cross-correlation between two correlation functions: velocity to GDI–Cdc42 interaction (using GDI.Cdc42 FLARE) and velocity to Cdc42 activity (using meroCBD) (**Fig. 2c**). As expected, these two functions correlated strongly and negatively, with a time lag of ~45 s at the leading edge (0–0.9 μm); that is, the reduction in GDI–Cdc42 interaction preceded the activation of the Cdc42 signal by ~45 s. In locations farther away from the cell edge, the strength of negative cross-correlation increased while the time lag converged to zero or even slightly positive values. This suggested a reduction in the time between Cdc42 release and activation with greater distance from the cell edge. However, we could not quantify the exact reduction in time lag because the positive lobe in the correlation function for velocity versus GDI–Cdc42 interaction at positive lag times biased the position of the cross-correlation minimum. Overall, these results showed that the new GDI.Cdc42 FLARE biosensor reported signals that were tightly coordinated with the activation of Cdc42 and the relationship between GDI–Cdc42 complex localization and Cdc42 activation.

Re-engineering a Cdc42 biosensor for multiplexed imaging

To analyze the relationship between localization of the GDI–Cdc42 complex and Cdc42 activation more directly, we strived for concurrent imaging of both events in the same cell. Our previously described meroCBD biosensor[6] is based on a fragment of the Wiskott–Aldrich syndrome protein (WASP) that binds selectively to active Cdc42. We covalently derivatized this fragment with mero87 dye, the fluorescence of which changes in response to changes in the solvent environment[29]. Dye fluorescence increased when the WASP fragment bound active Cdc42, revealing Cdc42 activation dynamics. Previously, enhanced green fluorescent protein (eGFP) was attached to this biosensor to enable 'ratio imaging', a technique for eliminating effects of cell morphology, biosensor concentration or uneven illumination on biosensor readouts[6]. eGFP wavelengths overlap those of the GDI.Cdc42 FLARE biosensor, so for the current study we replaced eGFP with maltose-binding protein (a nonfluorescent protein that enhances water solubility as eGFP does) and site-specifically labeled the biosensor with Atto 700 dye for ratio imaging (taking advantage of selective deprotonation of the WASP fragment N terminus at pH 5.2; **Supplementary Fig. 8a**). We attached the mero87 dye[6,29] selectively to a cysteine inserted at position 271 in the WASP fragment[6] using a cysteine-selective iodoacetamido derivative (neither the maltose-binding protein nor the WASP domain had other exposed cysteines). The two dyes attached with a 1:1 ratio and labeling efficiencies of >95%.

The mero87 dye on the new meroCBD biosensor showed a 325% increase in fluorescence after binding to Cdc42 (**Supplementary Fig. 8b**). The Atto 700 emission at 705 nm increased by 162%, enabling ratiometric measurements of Cdc42 activation (200% change in the ratio of mero87 emission to Atto 700 emission). The 705-nm emission of the Atto dye not only eliminated bleed-through into the CFP–YFP FRET channels but also was compatible with the laser-autofocus systems used in several commercial imaging systems. The Atto 700 dye showed photostability superior to that of other dyes used previously (**Supplementary Fig. 8c**).

Dynamics of Cdc42 activation and GDI–Cdc42 localization

To study the relative dynamics of Cdc42 activation and the localization of GDI–Cdc42 complex in the same cell, we microinjected the modified meroCBD biosensor into Swiss 3T3 MEFs stably expressing the GDI.Cdc42 FLARE biosensor. Although each biosensor could be used at effective concentrations without altering motility[6], we observed effects on cell morphology as well as reduced adhesion when we used similar concentrations of the two biosensors[26,27]. At concentrations where we observed no perturbation, low signal-to-noise ratios precluded correlation analysis. Therefore, we included a T35S mutation in the GDI.Cdc42 FLARE biosensor to reduce effector binding and enable the use of higher biosensor concentrations without changes in cell behavior. This mutation has the potential to generate dominant negative effects, so we stably expressed the T35S GDI.Cdc42 biosensor in MEFs under control of the tet-OFF system[30] and sorted the MEFs by flow cytometry on the basis of GDI.Cdc42 FLARE brightness before injection. We determined brightness levels that did not perturb normal motile behavior or Cdc42 activation dynamics (**Supplementary Fig. 9**).

Co-imaging of the T35S GDI.Cdc42 FLARE and meroCBD biosensors in living fibroblasts showed a relatively homogeneous distribution of low Cdc42 activity corresponding with elevated GDI–Cdc42 binding throughout most of the cell. This was consistent with the data generated with the non-T35S sensor, as well as with the notion of GDI maintaining a pool of inactive Cdc42 (**Fig. 3a**). Again, we observed transient and localized changes in the GDI–Cdc42 complex at the cell edge (**Fig. 3a**,**b**, **Supplementary Videos 5**–**7**), especially in regions with active retraction and protrusion. As with the non-T35S GDI.Cdc42 FLARE sensor, cross-correlation of the T35S GDI.Cdc42 FLARE signal with cell edge velocity consistently yielded a negative peak in all window rows between 0 and 4 μm from the cell edge (**Fig. 3c**), which was probably associated with the release of Cdc42 from GDI during protrusion events. Data from the GDI.Cdc42 FLARE biosensors and the T35S mutant biosensors differed quantitatively, but not qualitatively, in the time lag of this peak, suggesting that the two biosensors had somewhat different kinetics owing to the influence of effector binding. Moreover, the mutant sensor did not produce a significant positive correlation peak with respect to the velocity at positive time lags either at the cell edge or farther inside the cell (**Figs. 2c** and **3c**). Most probably, this secondary correlation peak disappeared because the absence of effector binding changed the dynamics of GDI–Cdc42 complex formation before protrusion events, or because the higher noise level masked more subtle secondary effects detected by the non-T35S sensor.

Figure 3b shows Cdc42 activation and GDI–Cdc42 localization observed by concurrent imaging of both FRET sensors during a representative episode of protrusion–retraction–protrusion. As predicted by the computational multiplexing analysis using GDI.Cdc42 FLARE, these data show a strong reduction in Cdc42 signal during protrusion. Moreover, decreases in amounts of GDI–Cdc42 complex accompanied Cdc42 activation as reported by the reengineered meroCBD. During retraction, we observed the opposite: Cdc42

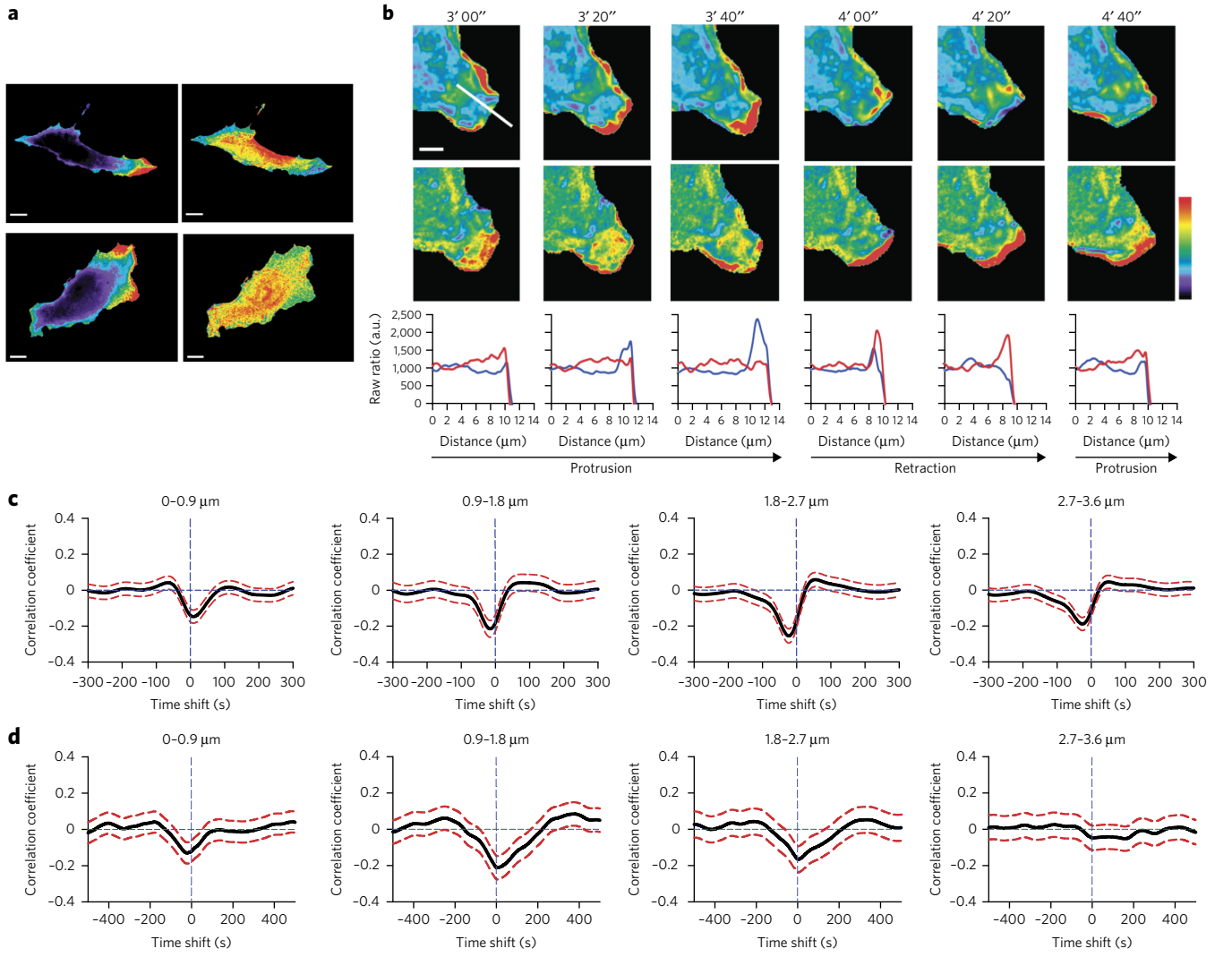

Figure 3 | Relationship between Cdc42 activation and GDI–Cdc42 localization monitored in the same cell. (**a**) MEFs expressing the T35S mutant version of the GDI.Cdc42 FLARE biosensor and injected with the modified meroCBD biosensor. Left, Cdc42 activity; right, GDI–Cdc42 localization. Pseudocolor scales: for Cdc42, black denotes 1.0, red denotes 7.46 (top row) or 2.82 (bottom row); for GDI–Cdc42, black denotes 1.0, red denotes 1.51 (top row) or 1.97 (bottom row). Scale bars, 20 μm. (**b**) Cdc42 activation (top row) and GDI–Cdc42 localization (middle row) in the same cell over time. Pseudocolor scales, from black to red: Cdc42, 1.0–2.3; GDI–Cdc42, 1.0–1.53. Scale bar, 5 μm. Bottom row: profile of Cdc42 activation (blue) and GDI–Cdc42 localization (red) along the diagonal white line shown in the leftmost panel of the top row. (**c**) Correlation of GDI–Cdc42 and edge velocity, measured using the T35S mutant GDI.Cdc42 FLARE biosensor. Correlation curves were computed from n = 886 individual windows in seven cells. (**d**) Correlation of Cdc42 activity and GDI–Cdc42 localization monitored in the same cell, using T35S mutant GDI.Cdc42 FLARE and the modified meroCBD biosensor. Correlation curves were computed from n = 420 individual windows in seven cells.

activation decreased, whereas amounts of localized GDI–Cdc42 complex sharply increased. This suggested that GDI promptly and efficiently sequestered deactivated Cdc42 during retraction. The profiles in **Figure 3b** also show that these inverse relations between Cdc42 activity and GDI–Cdc42 binding were concentrated at the very leading edge of a cell.

To quantify the coupling between Cdc42 activity and localization of the GDI–Cdc42 complex, we again applied correlation analysis. By simultaneously imaging both biosensors, we were able to map the spatial organization of the relationship between Cdc42 activation and GDI–Cdc42 complex formation. In sampling windows immediately adjacent to the cell edge, the correlation function showed a significant negative peak (P = 0.0204, t-test of H_0: correlation peak = 0) with a time lag of approximately −20 s, indicating that GDI released Cdc42 prior to Cdc42 activation (**Fig. 3d**). Qualitatively, this time lag between release and activation of the GTPase matched the GTPase-activation delay predicted by computational multiplexing (**Fig. 2c**). Also consistent between these two analyses, the negative peaks of the correlation function moved to zero in sampling windows 0.9–1.8 μm and 1.8–2.7 μm from the cell edge. As before, these data were consistent with concentration of active Cdc42–GEFs a few micrometers behind the cell edge, a proposition we made previously based on the cross-correlation between Cdc42 activity and velocity alone[4]. Contrary to the predictions made on the basis of computational multiplexing, which suggested a significant inverse relationship between Cdc42 activity and GDI–Cdc42 localization in sampling windows 2.7–3.6 μm from the cell edge, correlation analysis after simultaneous imaging of the two biosensors indicated that GDI–Cdc42 binding did not have a significant influence on the regulation of Cdc42 in regions more than ~3 μm from the cell edge. Again, this might have been due to the elimination of effector binding in the mutant biosensor, but overall these analyses showed that in qualitative terms the mutant T35S biosensor and the GDI.Cdc42 FLARE biosensor reported the same spatiotemporal coordination

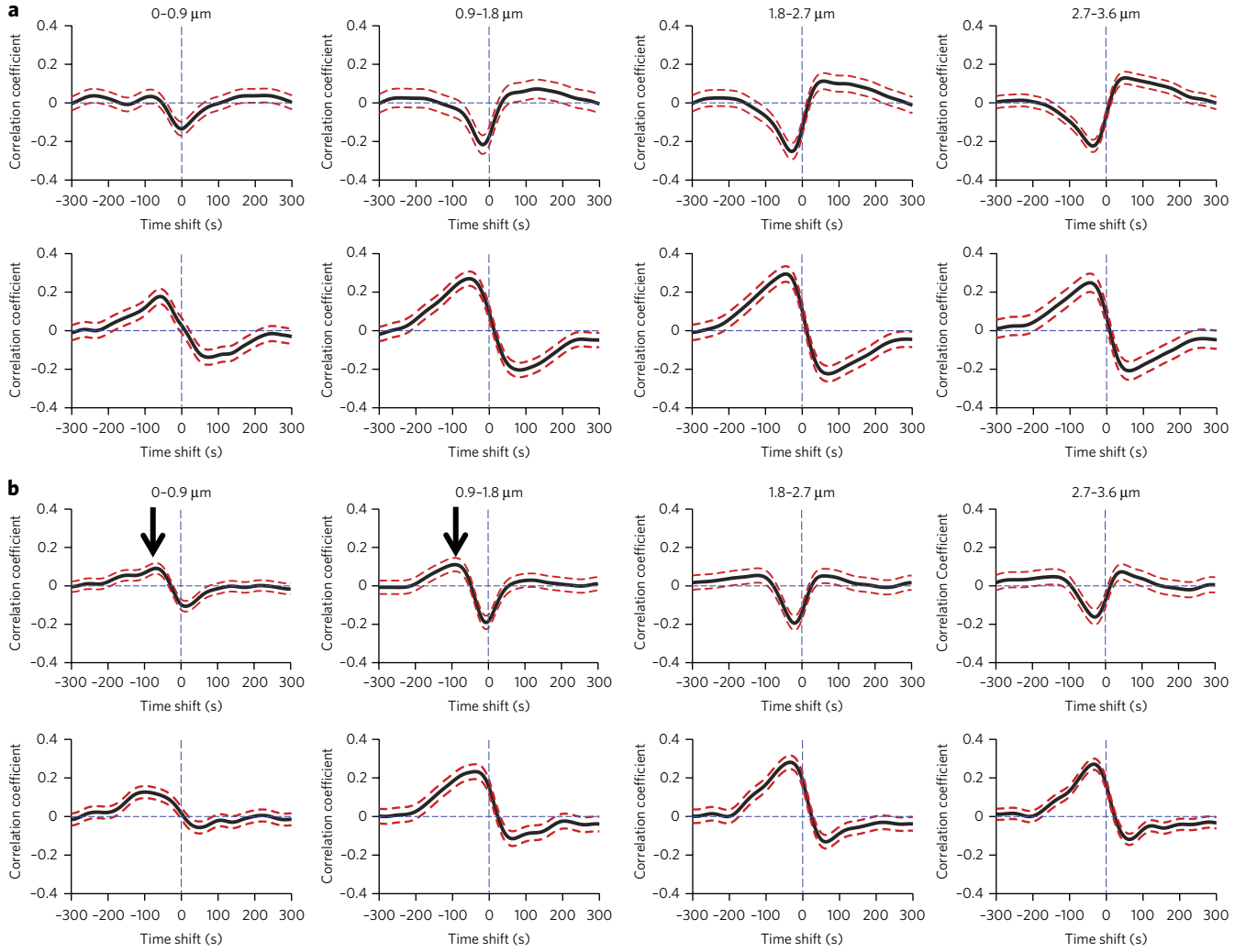

Figure 4 | Src-mediated phosphorylation of GDI at Y156 regulates the coordination of GDI–Cdc42 localization and Cdc42 activity in regions close to the edge. (**a**) A phosphorylation-deficient mutant of GDI (Y156F) had no effect on the timing of Cdc42 activation or modulation of GDI–Cdc42 localization. Top row: correlation of GDI–Cdc42 and edge velocity, using the T35S mutant GDI.Cdc42 FLARE biosensor expressed in cells containing Y156F GDI. Correlation curves were computed from n = 902 individual windows in 11 cells. Bottom row: correlation of Cdc42 activity and edge velocity using the meroCBD biosensor in cells containing Y156F GDI. Correlation curves are computed from n = 373 individual windows from five cells. (**b**) A phosphomimetic mutant of GDI (Y156E) produced positive correlation with edge velocity at negative time lags (i.e., after protrusion onset) similar to those of the correlation maxima of Cdc42 activity with edge velocity in regions close to the edge (0–1.8 μm). Top row: cross-correlation of GDI–Cdc42 and edge velocity using the T35S mutant GDI.Cdc42 FLARE biosensor expressed in cells containing Y156E GDI. Correlation curves were computed from n = 979 individual windows from 11 cells. Black arrows in regions 0–1.8 μm from the edge indicate the appearance of a positive cross-correlation peak in GDI–Cdc42 complex localization. Bottom row: cross-correlation of Cdc42 activity and edge velocity using the meroCBD biosensor in cells containing Y156E GDI. Correlation curves were computed from n = 491 individual windows in four cells.

of GDI binding and GTPase activation, and that the antenna can be used with dye-based biosensors for multiplexed imaging.

Src regulation of GDI–Cdc42 interaction

Equipped with tools enabling us to directly observe and quantify the relationships between GDI–Cdc42 complex and Cdc42 activation, we sought to validate and expand biochemical models of the regulation of GDI–GTPase interactions in the context of living cells. Previous biochemical studies showed that phosphorylation of GDI by Src at Y156 largely abolishes GDI's affinity for Cdc42, Rac1 and RhoA[15]. Moreover, this phosphorylation affects the ability of GDI to extract RhoA from isolated plasma membrane[15]. Thus, Src may regulate the localization and timing of GDI–Cdc42 interactions during protrusion. To test this in living cells, we established an optimized knockdown/rescue procedure to replace endogenous GDI with either Y156F (phosphorylation-deficient) or Y156E (phosphomimetic) GDI and examined the effects of these changes on the leading edge correlations (**Fig. 4**). The Y156F GDI mutant has a cellular distribution and phenotype similar to that of the wild-type GDI, whereas Y156E GDI accumulates at the leading cell edge and within edge ruffles[15]. Although such accumulation has been observed in fixed cells, *in vivo* evidence for binding of Y156E GDI to Cdc42 at the edge ruffles in living cells remains elusive, especially in light of the severely abrogated affinity of the Y156E GDI mutant for GTPases[15]. We used short hairpin RNA (shRNA) against endogenous GDI (**Supplementary Figs. 10** and **11**) followed by stable viral transduction with GDI mutants resistant to the shRNA[2,15,31]. For these experiments we used the T35S GDI.Cdc42.FLARE biosensor to probe GDI–Cdc42 localization and imaged Cdc42 activity in separate cells to avoid overloading cells harboring GDI mutations with two biosensors (**Supplementary Videos 8–11**). As expected, cross-correlations between edge motion and Cdc42 activity in cells

with Y156F GDI were identical to those observed with wild-type GDI (**Figs. 2c** and **4a**). In contrast, Y156E GDI produced a small but measureable positive cross-correlation between GDI binding and edge motion at negative time lags for the two window rows closest to the cell edge (**Fig. 4b**). On the basis of this observation, we concluded that at these locations the mutant GDI bound to plasma-membrane-localized Cdc42 and was thus confined within its activation compartment. Previous observations from immunofluorescence experiments[15] show accumulation of Y156E GDI in this region, supporting the notion that the reduced affinity of this mutant GDI for GTPase prevents transfer of the prenylated C terminus of the GTPase out of the plasma membrane and into the β-sandwich of the GDI structure. Hence, this mutation may prevent extraction of the GTPase from the plasma membrane. Our results here showed that a substantial fraction of GDI actually bound and remained bound to Cdc42 at the edge, probably because of its reduced affinity. At distances farther from the cell edge, the correlation functions were qualitatively the same as those of the nonmutant biosensor (**Fig. 4b**). This indicated that activation of Cdc42 and localization of the Cdc42–Y156E GDI complex were concurrent or concomitant only in the edge region (0–1.8 μm from the cell edge). Furthermore, the formation of GDI–Cdc42 complex and Cdc42 activation at those locations occurred with the same dynamics (**Fig. 4b**). Both lagged behind changes in protrusion velocity (Cdc42 (0–0.9 μm), −87 ± 47.5 s; GDI binding (0–0.9 μm), −67 ± 28 s; *t*-test comparing Cdc42 activation and GDI binding at 0–0.9 μm, $P = 0.358425$; Cdc42 (0.9–1.8 μm), −45 ± 42.5 s; GDI binding (0.9–1.8 μm), −92 ± 40.5 s; *t*-test comparing Cdc42 activation and GDI binding at 0.9–1.8 μm, $P = 0.21733$). As in previous observations, the Y156E GDI mutant produced slightly faster leading edge turnover rates[15] (**Supplementary Fig. 5**). Together, these data demonstrate that in living cells, phosphorylation of GDI at Y156 by Src regulated not the ability of GDI to bind to GTPase but rather the ability of GDI to extract GTPases from the plasma membrane.

DISCUSSION

We have described an approach to sense protein interaction in living cells by modifying only one of two interacting proteins. A binding antenna was placed on Rho GTPases where its FRET was affected by GDI binding but not by other ligands. Use of a binding antenna can substantially reduce cell perturbation because only one protein in an interacting pair needs modification. Attaching binding antennae to affinity reagents that interact selectively with activated target proteins (for example, the WASP domain in the meroCBD biosensor used here) should make it possible to construct genetically encoded biosensors that sense the activation of endogenous proteins.

Through multiplexed imaging of GDI–Cdc42 interaction and Cdc42 activation, we determined the relative kinetics of these two events in the context of cell protrusions. We show that localized buildups of GDI–Cdc42 complex and Cdc42 activation were inversely related within protrusions. Mapping of this relationship showed remarkably tight coordination on a time scale of 10 s. This suggests that GDI–Cdc42 interactions are a critical component in the spatiotemporal regulation of Cdc42 activity, and not merely a mechanism for global sequestration of an inactive pool of GTPase. Extrapolation from the time scale of cell protrusion suggests that regulation of GDI–Cdc42 interaction may in fact be rate limiting in GTPase activation during this process: after the release of signaling molecules into the plasma membrane, sufficient GEFs are already primed or rapidly activated to induce GDP-to-GTP exchange on a time scale of seconds. It would follow that the characteristic timing of Cdc42 activation during protrusion events is mediated at least in part by localized release of GTPase from GDI. Indeed, the cross-correlation between the appearance of the GDI–Cdc42 complex and edge velocity showed a remarkably narrow spike over the time lag interval of ~25 s, suggesting that Cdc42 was released shortly after the protrusion edge velocity reached maximal values. The resulting positive correlation of Cdc42 with velocity stretched over a sixfold-longer time lag interval. This observation is again consistent with a mechanism in which GEFs rapidly activate Cdc42 at the protruding cell edge and the activated molecules then diffuse over a broader region in which they remain active through repeated interactions with GEFs or through diminished GAP activity. This example illustrates that understanding GTPase signaling will require correlation of the activity of GDI, GEFs and GAPs. With the present work, we have taken a first step in this direction.

Our spatiotemporal analysis of the GDI–Cdc42 complex also showed precisely localized decreases in GDI–Cdc42 complex concentrations. This was especially surprising for an interaction that has thus far been associated with global sequestration of GTPases. Although several cues could modulate the interaction, our findings now add to these data the requirement that the cues themselves operate with precise localization and timing. As proof of principle, we demonstrated here how the GDI–Cdc42 interaction responded to Src kinase activity, affecting the ability of GDI to extract GTPase from the plasma membrane. We picked Src from among the GDI-phosphorylating kinases because its activity is precisely coupled to the formation and force-mediated activation of adhesions[32,33], and because of its documented roles in GEF activation[34]. As other kinases could be specific for different GTPases[15–17,35], further investigation in this area using biosensors would be valuable.

In summary, our work proposes a hitherto unappreciated complexity in the regulation of Rho GTPase signaling activity. In addition to the well-established roles of GEFs and GAPs as spatiotemporal sculptors of the GTPase signaling landscape, this study points to GDI interactions as a factor. The described biosensor provides a valuable means to dissect these regulatory mechanisms in the context of diverse cell functions, and the antenna readout mechanism provides a tool for examining protein–protein interactions with modification of only one interacting partner.

Received 23 March 2015; accepted 16 May 2016;
published online 8 August 2016

METHODS

Methods and any associated references are available in the online version of the paper.

References

1. Jaffe, A.B. & Hall, A. Rho GTPases: biochemistry and biology. *Annu. Rev. Cell Dev. Biol.* **21**, 247–269 (2005).
2. Garcia-Mata, R., Boulter, E. & Burridge, K. The 'invisible hand': regulation of RHO GTPases by RHOGDIs. *Nat. Rev. Mol. Cell Biol.* **12**, 493–504 (2011).
3. Lawson, C.D. & Burridge, K. The on-off relationship of Rho and Rac during integrin-mediated adhesion and cell migration. *Small GTPases* **5**, e27958 (2014).
4. Machacek, M. *et al.* Coordination of Rho GTPase activities during cell protrusion. *Nature* **461**, 99–103 (2009).
5. Pertz, O., Hodgson, L., Klemke, R.L. & Hahn, K.M. Spatiotemporal dynamics of RhoA activity in migrating cells. *Nature* **440**, 1069–1072 (2006).
6. Nalbant, P., Hodgson, L., Kraynov, V., Toutchkine, A. & Hahn, K.M. Activation of endogenous Cdc42 visualized in living cells. *Science* **305**, 1615–1619 (2004).
7. Tsukada, Y. *et al.* Quantification of local morphodynamics and local GTPase activity by edge evolution tracking. *PLoS Comput. Biol.* **4**, e1000223 (2008).
8. Kurokawa, K. & Matsuda, M. Localized RhoA activation as a requirement for the induction of membrane ruffling. *Mol. Biol. Cell* **16**, 4294–4303 (2005).
9. Itoh, R.E. *et al.* Activation of rac and cdc42 video imaged by fluorescent resonance energy transfer-based single-molecule probes in the membrane of living cells. *Mol. Cell. Biol.* **22**, 6582–6591 (2002).
10. Cherfils, J. & Zeghouf, M. Regulation of small GTPases by GEFs, GAPs, and GDIs. *Physiol. Rev.* **93**, 269–309 (2013).
11. Chuang, T.H., Bohl, B.P. & Bokoch, G.M. Biologically active lipids are regulators of Rac.GDI complexation. *J. Biol. Chem.* **268**, 26206–26211 (1993).
12. Del Pozo, M.A. *et al.* Integrins regulate GTP-Rac localized effector interactions through dissociation of Rho-GDI. *Nat. Cell Biol.* **4**, 232–239 (2002).

13. Ugolev, Y., Berdichevsky, Y., Weinbaum, C. & Pick, E. Dissociation of Rac1(GDP).RhoGDI complexes by the cooperative action of anionic liposomes containing phosphatidylinositol 3,4,5-trisphosphate, Rac guanine nucleotide exchange factor, and GTP. *J. Biol. Chem.* **283**, 22257–22271 (2008).
14. Michaelson, D. *et al.* Differential localization of Rho GTPases in live cells: regulation by hypervariable regions and RhoGDI binding. *J. Cell Biol.* **152**, 111–126 (2001).
15. DerMardirossian, C., Rocklin, G., Seo, J.Y. & Bokoch, G.M. Phosphorylation of RhoGDI by Src regulates Rho GTPase binding and cytosol-membrane cycling. *Mol. Biol. Cell* **17**, 4760–4768 (2006).
16. Dovas, A. *et al.* Serine 34 phosphorylation of rho guanine dissociation inhibitor (RhoGDIalpha) links signaling from conventional protein kinase C to RhoGTPase in cell adhesion. *J. Biol. Chem.* **285**, 23296–23308 (2010).
17. DerMardirossian, C., Schnelzer, A. & Bokoch, G.M. Phosphorylation of RhoGDI by Pak1 mediates dissociation of Rac GTPase. *Mol. Cell* **15**, 117–127 (2004).
18. Lang, P. *et al.* Protein kinase A phosphorylation of RhoA mediates the morphological and functional effects of cyclic AMP in cytotoxic lymphocytes. *EMBO J.* **15**, 510–519 (1996).
19. Tkachenko, E. *et al.* Protein kinase A governs a RhoA-RhoGDI protrusion-retraction pacemaker in migrating cells. *Nat. Cell Biol.* **13**, 660–667 (2011).
20. Ellerbroek, S.M., Wennerberg, K. & Burridge, K. Serine phosphorylation negatively regulates RhoA in vivo. *J. Biol. Chem.* **278**, 19023–19031 (2003).
21. Forget, M.A., Desrosiers, R.R., Gingras, D. & Beliveau, R. Phosphorylation states of Cdc42 and RhoA regulate their interactions with Rho GDP dissociation inhibitor and their extraction from biological membranes. *Biochem. J.* **361**, 243–254 (2002).
22. Rizzo, M.A. & Piston, D.W. High-contrast imaging of fluorescent protein FRET by fluorescence polarization microscopy. *Biophys. J.* **88**, L14–L16 (2005).
23. Nagai, T., Yamada, S., Tominaga, T., Ichikawa, M. & Miyawaki, A. Expanded dynamic range of fluorescent indicators for Ca^{2+} by circularly permuted yellow fluorescent proteins. *Proc. Natl. Acad. Sci. USA* **101**, 10554–10559 (2004).
24. Yang, F., Moss, L.G. & Phillips, G.N. Jr. The molecular structure of green fluorescent protein. *Nat. Biotechnol.* **14**, 1246–1251 (1996).
25. DerMardirossian, C. & Bokoch, G.M. GDIs: central regulatory molecules in Rho GTPase activation. *Trends Cell Biol.* **15**, 356–363 (2005).
26. White, M.A. *et al.* Multiple Ras functions can contribute to mammalian cell transformation. *Cell* **80**, 533–541 (1995).
27. Ellis, S. & Mellor, H. The novel Rho-family GTPase Rif regulates coordinated actin-based membrane rearrangements. *Curr. Biol.* **10**, 1387–1390 (2000).
28. Takai, Y. *et al.* Rho small G protein and cytoskeletal control. *Princess Takamatsu Symp.* **24**, 338–350 (1994).
29. Toutchkine, A., Nguyen, D.V. & Hahn, K.M. Merocyanine dyes with improved photostability. *Org. Lett.* **9**, 2775–2777 (2007).
30. Gossen, M. & Bujard, H. Tight control of gene expression in mammalian cells by tetracycline-responsive promoters. *Proc. Natl. Acad. Sci. USA* **89**, 5547–5551 (1992).
31. Boulter, E. *et al.* Regulation of Rho GTPase crosstalk, degradation and activity by RhoGDI1. *Nat. Cell Biol.* **12**, 477–483 (2010).
32. Wang, Y. *et al.* Visualizing the mechanical activation of Src. *Nature* **434**, 1040–1045 (2005).
33. Galbraith, C.G., Yamada, K.M. & Sheetz, M.P. The relationship between force and focal complex development. *J. Cell Biol.* **159**, 695–705 (2002).
34. Aghazadeh, B., Lowry, W.E., Huang, X.Y. & Rosen, M.K. Structural basis for relief of autoinhibition of the Dbl homology domain of proto-oncogene Vav by tyrosine phosphorylation. *Cell* **102**, 625–633 (2000).
35. Qiao, J. *et al.* Phosphorylation of GTP dissociation inhibitor by PKA negatively regulates RhoA. *Am. J. Physiol. Cell Physiol.* **295**, C1161–C1168 (2008).

Acknowledgments

We thank the National Institute of General Medical Sciences (P01-GM103723 and T-R01 GM090317 to G.D. and K.M.H.; GM099837 to C.D.) and the National Cancer Institute (CA181838 to L.H.) for funding. O.D. is a Howard Hughes Medical Institute International Student Research Fellow. Mammalian expression cDNA constructs for Myc-WASP and HA-Tiam1 were gifts from D. Cox (Departments of Anatomy and Structural Biology and Developmental and Molecular Biology, Albert Einstein College of Medicine, Bronx, New York, USA). Myc-Intersectin1L was a gift from H. Bourne (Department of Cellular and Molecular Pharmacology, University of California, San Francisco, San Francisco, California, USA). Myc-mDia2 was from S. Narumiya (Department of Pharmacology, University of Kyoto, Kyoto, Japan). PAK1 was from Y. Wu (Department of Genetics and Genome Sciences, University of Connecticut Health Center, Farmington, Connecticut, USA).

Author contributions

L.H. and K.M.H. conceived the biosensor; L.H. optimized and built the biosensor; L.H., D.S. and G.D. designed and interpreted correlation experiments; L.H. and D.S. performed biological experiments; M.S.-G. and L.H. performed the computational analysis; O.D. and K.M.H. performed structural analysis and interpreted studies to examine the antennae mechanism; C.D. subcloned the shRNA expression constructs and gave critical feedback; and L.H., G.D. and K.M.H. wrote the manuscript with input from all other authors.

Competing financial interests

The authors declare no competing financial interests.

Additional information

Any supplementary information, chemical compound information and source data are available in the online version of the paper. Reprints and permissions information is available online at http://www.nature.com/reprints/index.html. Correspondence and requests for materials should be addressed to L.H., G.D. or K.M.H.

ONLINE METHODS

Biosensor expression constructs. We cloned the GDI.Cdc42 FLARE biosensor by connecting a hexaHis tag, a monomeric Cerulean FP[22] and a circularly permutated (cp49) Venus FP[23]. Monomeric Cerulean and cp49 Venus FPs were connected by a GSGS linker, which was flanked by HindIII and NotI restriction sites on the 5′ and 3′ ends, respectively. The construct was cloned into a pTriEX-HisMyc4 backbone (Novagen) at NcoI/EcoRI sites. RhoGTPases were cloned by PCR using primer sets 5′-CCAAGGAATTCATGGCTGCCATCCGGAAG-3′ and 5′-GGTGATGGTGGTGCTCGAGTTATCACAAGAC-3′ for RhoA, 5′-CAAGGAATTCATGCAGGCCATCAAGTGTGTGG-3′ and 5′-GGTGATGGTGGTGCTCGAGTTATTACAACAGC-3′ for Rac1, and 5′-CCCCCGGAATTCATGCAGACAATTAAGTGTG-3′ and 5′-GGTGATGGTGGTGCTCGAGTTATCATAGCAG-3′ for Cdc42. Primers encoded an EcoRI site at the 5′ end of the fragment and an XhoI site after the stop codon on the 3′ end. They were inserted in-frame at the C terminus of the Antenna module in the pTriEx-HisMyc4 backbone. We used the Quikchange mutagenesis kit (Stratagene) to introduce point mutations into the fragment encoding the GTPase, producing different mutant versions of the biosensor. To produce the tetracycline-inducible retroviral construct, we cut out the cDNA encoding the GDI biosensor as a single cassette using NcoI/XhoI sites, blunt-ended it using an end-filling reaction using DNA Polymerase I Large (Klenow) fragment (New England Biologicals) and blunt-end ligated it into the multiple cloning site at HpaI in the pBabe-sin-Puro-tet-CMV backbone[36]. We used the GP2-293 cell line (purchased from Clontech and tested for mycoplasma by PCR) to produce the pantropic retrovirus by cotransfecting the pVSVg vector (Clontech). We cultured infected MEFs that stably expressed the tetracycline transactivating element (tet-OFF MEF/3T3; purchased from Clontech and tested for mycoplasma by PCR) in DMEM supplemented with 10% FBS. We selected the cultured cells for stable incorporation of the biosensor by puromycin treatment (10 μg/ml) and sorted them by flow cytometry to collect cell fractions expressing different levels of the biosensor. Doxycycline (10 μg/ml) was maintained in the culture medium to repress the expression of biosensor during normal cell culture. Forty-eight hours before imaging experiments, we removed doxycycline by detaching cells via brief trypsinization and replating them into fresh culture medium at 10^{-4} cells per 10-cm tissue culture dish.

Western blotting, reagents and antibodies. We prepared whole-cell lysates by lysing cells in ice-cold NP-40 lysis buffer (150 mM NaCl, 1.0% NP-40, 50 mM Tris-Cl, pH 8.0) with protease inhibitor cocktail (Sigma). Lysates were resolved by SDS–PAGE and transferred to PVDF membrane. After blocking in 5% BSA in TBST, blots were incubated overnight at 4 °C in primary antibody at 1:1,000 dilution followed by secondary antibody at 1:10,000 dilution. Blots were analyzed using the Odyssey Infrared Imaging System (LI-COR). For quantification, the integrated values of background-corrected band densities were measured with Metamorph software (Molecular Devices). The following primary antibodies were used for the western blotting analysis and immunofluorescence: mouse monoclonal anti-RhoA (Santa Cruz Biotechnology, clone 26C4), mouse monoclonal anti-Rac1 (Millipore, clone 23A8), rabbit polyclonal anti-Cdc42 (Millipore; 07-1466), rabbit polyclonal anti–GDI-α (Santa Cruz Biotechnology, A-20; sc-360), mouse monoclonal anti–β-actin (Santa Cruz Biotechnology, clone AC-15), mouse monoclonal anti-HA (Covance, clone 16B12), mouse monoclonal anti-Myc (Cell Signaling, clone 9B11), rabbit polyclonal anti-Src pY418 (Invitrogen; 44-660G), mouse monoclonal anti-Src (Millipore, clone GD11) and mouse monoclonal anti-GFP (Roche, clones 7.1 and 13.1). Secondary antibodies included the following: goat anti-mouse IRDye800CW (LI-COR; 926-32210), goat anti-rabbit IRDye800CW (LI-COR; 926-32211), goat anti-mouse conjugated to Alexa Fluor 594 (Invitrogen; A-11005), and donkey anti-rabbit IRDye680LT (LI-COR; 926-68023). Mammalian expression cDNA constructs for MYC–WASP and HA–TIAM1 were gifts from Dr. Dianne Cox (Albert Einstein College of Medicine). MYC-Intersectin1L was a gift from Dr. Henry Bourne (University of California, San Francisco). MYC-mDia2 was from Dr. Shuh Narumiya (University of Kyoto). PAK1 was from Dr. Yi Wu (University of Connecticut Health Center).

***In vitro* fluorometry assay.** We carried out fluorometry assays according to published protocols[5]. Briefly, in experiments in which the biosensor was cotransfected with negative regulators (GDI or GAP), the ratio of biosensor to regulator cDNA was 1:4. In experiments using GEFs with excess GDI, the DNA ratio for biosensor:RhoGDI:GEF was 1:4:1–5. In experiments with GEFs and GAP without excess GDI, the ratio of biosensor to regulator cDNA was 1:4. In experiments with effectors, the biosensor:effector DNA ratio was 1:4. The total amount of transfected DNA was kept to 4–5 μg per well in a six-well plate, using a total fluid volume of 2 ml per well. HEK 293T (purchased from ATCC and tested for mycoplasma by PCR) cells were plated in six-well plates overnight at 1.25×10^{-6} cells per well. DNA was transfected using the Lipofectamine 2000 reagent (Invitrogen) according to the manufacturer's protocols. Forty-eight hours after transfection, cells were trypsinized, detached and suspended in cold PBS. The cell suspension was immediately measured in a Fluorolog SPEX MF2 spectrofluorometer (Horiba Jobin Yvon). Emission was measured from 450 to 600 nm, with 433-nm excitation. Emission counts at 525 nm were then divided by the emission counts at 470 nm to normalize for biosensor concentration.

shRNA knockdown/rescue. The shRNA used for GDI was as designed previously[15]. cDNA encoding the shRNA (and a scrambled control) (5′-TGCGCGCTATGTAGGATTCGTTCAAGAGACGAATCCTACATAGCGCGCTTTTTTC-3′) was cloned into pLL5.5CMV[37] at HpaI/XhoI sites. Lentivirus incorporating the shRNA expression construct was produced using the GP2-293 packaging cell line together with the pVSVg envelope system according to the manufacturer's protocols (Clontech). To produce efficient knockdown and rescue using the shRNA-resistant versions of wild-type and mutant GDI[15], we used a retroviral expression system to stably incorporate the Y156E and Y156F mutant versions of GDI using the pQCXIH system (Clontech) and selected with 100 μg/ml hygromycin B. In the endogenous wild-type GDI background, stable expressions of these mutant versions of GDI did not seem to affect cell health. For the production of wild-type GDI knockdown/rescue, we used a pRetro-X-Hygro backbone (Clontech) to suppress the expression of the wild-type GDI using the tet-OFF system. MEFs stably incorporating the GDI biosensor were plated onto tissue culture dishes plated with poly-L-lysine and allowed to induce expression of the biosensor for 48 h through the removal of doxycycline. Lentivirus containing the shRNA for GDI was applied, and, for most effective knockdown efficiency, the cells were allowed to recover for 96 h before imaging experiments.

Microscopy and live-cell imaging. To quantify the activity of two biosensors in the same cell, we combined the GDI.Cdc42 FLARE biosensor, based on CFP–YFP FRET, with a modification of the meroCBD Cdc42 biosensor[4,6]. We altered the wavelengths of meroCBD to produce fluorescence orthogonal to that of GDI.Cdc42 FLARE by using a version of the far-red dye Atto 700 NHS (Sigma) with improved photostability. We also removed the eGFP from meroCBD because of spectral overlap between eGFP and the CFP–YFP FRET pair in GDI.Cdc42 FLARE. Removal of the GFP greatly reduced the water solubility of the dye-labeled CBD domain, so we attached maltose-binding protein to the C terminus of CBD using a GSGSGS linker. The N-terminal amine of the CBD–maltose-binding protein construct was labeled site-specifically with Atto 700 NHS succinimidyl ester at pH 5.6. Modification of the original meroCBD biosensor was prompted by two factors: (1) photobleacing of the original Alexa Fluor 750 (Invitrogen) dye was very fast, and (2) our multi-channel imaging system[38] used a laser-based autofocus system that precluded the use of wavelengths above 750 nm.

MEF/3T3 cells induced to express the GDI biosensor by removal of tetracycline were plated directly on glass coverslips for 5–6 h before microinjection and imaging. Coverslips were cleaned by ultrasonication and were then soaked in 70% ethanol before use in these studies. Modified meroCBD was microinjected and cells were allowed to recover for 30 min before imaging. Cells were imaged in Ham's F-12K medium without phenol red (Biosource) sparged with argon to remove dissolved oxygen and supplemented with 3% FBS, 10 mM HEPES, 10 μg/ml Oxyfluor reagent (Oxyrase Inc.) and 10 mM DL-lactate. Cells were imaged at 37 °C in a closed chamber. Images were obtained using a 40×/1.3–numerical aperture (NA) PLANAPO UIS2 DIC objective (Olympus) and an IX81 ZDC inverted microscope (Olympus) with a beam splitter for simultaneous acquisition of both FRET and CFP channels using two CoolsnapESII CCD (charge-coupled device) cameras (Roper

Photometrics). For the acquisitions of mero87 and Atto 700 fluorescence, a CoolsnapHQ2 (Roper Photometrics) camera was attached to the bottom port of the microscope via a filterwheel that changed the emission filters between mero87 and Atto 700 emission wavelengths during acquisition at each time point. Metamorph software version 7.1.7 was used to control the microscope and acquire image sets at 10-s time intervals. The imaging system is described in detail elsewhere[38].

Image processing and analysis. Metamorph version 7.1.7 was used to perform image processing and data analysis. All images were flat-field corrected and background subtracted[39]. Both FRET/CFP and mero87/Atto 700 images were intensity-thresholded to generate a binary mask with a value of 0 outside the cell and a value of 1 inside the cell. Shading-corrected and background-subtracted images were multiplied by the corresponding binary masks to set areas outside the cell uniformly to zero, as well as to minimize noise and other artifacts. The resulting images were then aligned computationally using previously described procedures[40,41] to ascertain optimal registration with sub-pixel accuracy. Masked FRET or mero87 images were divided by the masked CFP or Atto 700 images, respectively, to yield a ratio reflecting GDI–GTPase interaction or Cdc42 activation. A linear pseudocolor lookup table was applied to the ratiometric images. In every data set, raw fluorescent images were carefully inspected to verify that all portions used to create the ratio image had sufficient signal-to-noise ratio. This was especially important in thin parts of the cell where fluorescence was low. In time-lapse experiments, various fluorophores bleached at different rates. We corrected the ratio for bleaching using a previously published method[42].

Cell edge tracking. Cell edges were derived from the binary mask mentioned above. The changing position of edges over time was tracked computationally with previously described software written in Matlab (Mathworks)[43]. We calculated rates of protrusion and retraction (velocity maps) using the finite differences of positions in consecutive frame triplets at $T-1$, T and $T+1$.

Definition of sampling windows. Because of the subcellular heterogeneity of protrusion and retraction states, relationships among GDI–Cdc42 binding, Cdc42 activation and cell edge motion had to be identified locally. As in previous work[4], we determined small probing windows 1–2 μm in width and 0.9 μm deep that moved with the edge (**Supplementary Fig. 6**). The width of the windows was set in agreement with the FWHM (full-width at half-maximum) of ~4 μm of the average spatial autocorrelation of edge velocity fluctuations along the cell edge; that is, along the cell edge, signaling and motion activity were sampled at Nyquist frequency or finer. The depth of the windows was set on the basis of previous studies that revealed changes in Cdc42 signaling away from the cell edge over distances as short as 1 μm (refs. 4,6). Windows were propagated over time such that they maintained a fixed geometric relationship with a particular location at the cell edge. For windows at the cell edge, protrusion/retraction vectors were averaged to report a mean velocity over the edge segment covered by a particular window. For all windows, the values of the normalized FRET values were averaged over all pixels contained by a particular window. This allowed the construction of space–time activity maps that were cell-shape invariant and amenable to statistical analysis of the temporal relations between the two signaling activities and edge motion.

Correlation analysis. Temporal cross-correlations between two variables sampled in a particular window were determined by Pearson's correlation coefficient. For windows located away from the cell edge, we calculated correlations between signaling activity and edge motion by extracting the time series of the former with the time series of the edge motion measured in the closest window located at the cell periphery. We obtained the correlation between two variables at a particular distance from the edge by averaging the correlation function over all sampling windows at the set distance.

To investigate the cell-to-cell heterogeneity of the cross-correlation, we estimated a common cross-correlation by computing a smoothing spline for the ensemble of average correlation data from different cells. We calculated the variance of the smoothing spline approximation, and hence of the location of the maximum correlation, using a nonparametric bootstrap method[44,45]: from the residuals of the approximated spline, we took 2,000 bootstrap samples to calculate local variation of the spline about the mean, variation in maximum correlation coefficient, and variation in location of the maximum correlation (time lag). We obtained the 95% confidence interval for the estimated common cross-correlation in each location as the interval containing 95% of the bootstrapped spline samples.

Representing the biosensor using crystal structure data. We constructed the hypothetical structure of the GDI.Cdc42 FLARE biosensor in **Supplementary Figure 4** using the crystal structures of Cdc42 in complex with GAP (PDB ID 2NGR), GEF (PDB ID 1KZ7) and GDI (PDB ID 1DOA). We used PyMOL software v1.7.4.4 (Schrödinger LLC) to visualize these structures and to edit the relative locations of FPs. We assumed cp49 Venus and Cerulean would form a dimer similar to the GFP wild-type dimer, which was used as a template (PDB ID 2B3Q) to show the dimer of cp49 Venus and Cerulean in the high-FRET state.

Statistical analysis. All P values were determined via Student's t-test. No statistical methods were used to pre-determine the sample size, and no randomizations were used. The investigators were not blinded to allocation during experiments or outcome assessment. Statistical tests used are stated in figure legends, along with P values as appropriate. Data distribution should meet the normal distribution requirements. No estimate of variation was made. No pre-established criteria were used to determine data inclusion or exclusion.

Code availability. Matlab codes are available upon request.

36. Morgenstern, J.P. & Land, H. Advanced mammalian gene transfer: high titre retroviral vectors with multiple drug selection markers and a complementary helper-free packaging cell line. *Nucleic Acids Res.* **18**, 3587–3596 (1990).
37. Cai, L., Marshall, T.W., Uetrecht, A.C., Schafer, D.A. & Bear, J.E. Coronin 1B coordinates Arp2/3 complex and cofilin activities at the leading edge. *Cell* **128**, 915–929 (2007).
38. Spiering, D. & Hodgson, L. Multiplex imaging of Rho family GTPase activities in living cells. *Methods Mol. Biol.* **827**, 215–234 (2012).
39. Hodgson, L., Shen, F. & Hahn, K. Biosensors for characterizing the dynamics of rho family GTPases in living cells. *Curr. Protoc. Cell Biol.* Chapter 14, Unit 14.11.1-26 (2010).
40. Spiering, D., Bravo-Cordero, J.J., Moshfegh, Y., Miskolci, V. & Hodgson, L. Quantitative ratiometric imaging of FRET-biosensors in living cells. *Methods Cell Biol.* **114**, 593–609 (2013).
41. Shen, F. *et al.* Functional proteometrics for cell migration. *Cytometry A* **69**, 563–572 (2006).
42. Hodgson, L., Nalbant, P., Shen, F. & Hahn, K. Imaging and photobleach correction of Mero-CBD, sensor of endogenous Cdc42 activation. *Methods Enzymol.* **406**, 140–156 (2006).
43. Machacek, M. & Danuser, G. Morphodynamic profiling of protrusion phenotypes. *Biophys. J.* **90**, 1439–1452 (2006).
44. Efron, B. & Tibshirani, R. *An Introduction to the Bootstrap* (Chapman & Hall, New York, 1993).
45. Efron, B. Bootstrap methods: another look at the jackknife. *Ann. Stat.* **7**, 1–26 (1979).

doi:10.1038/nchembio.2145